Clim. Past Discuss., 11, 5307–5343, 2015
www.clim-past-discuss.net/11/5307/2015/
doi:10.5194/cpd-11-5307-2015

Climate of the Past Discussions
Open Access
EGU

On the spatial and temporal variability of ENSO precipitation and drought teleconnection in mainland Southeast Asia

T. A. Räsänen[1], V. Lindgren[1], J. H. A. Guillaume[1], B. M. Buckley[2], and M. Kummu[1]

[1]Water & Development Research Group, Aalto University, Tietotie 1E, 02150 Espoo, Finland
[2]Tree Ring Laboratory, Lamont–Doherty Earth Observatory of Columbia University, 61 Route 9W, Palisades, NY, USA

Received: 14 October 2015 – Accepted: 26 October 2015 – Published: 10 November 2015

Correspondence to: T. A. Räsänen (timo.rasanen@aalto.fi)

Published by Copernicus Publications on behalf of the European Geosciences Union.

Abstract

The variability in the hydroclimate over mainland Southeast Asia is strongly influenced by the El Niño–Southern Oscillation (ENSO) phenomenon, which has been linked to severe drought and floods that profoundly influence human societies and ecosystems alike. However, the spatial characteristics and long-term stationarity of ENSO's influence in the region are not well understood. We thus aim to analyse seasonal evolution and spatial variations in the effect of ENSO on precipitation over the period of 1980–2013, and long-term variation in the ENSO-teleconnection using tree-ring derived Palmer Drought Severity Indices (PDSI) that span from 1650–2004. We found that the majority of the study area is under the influence of ENSO, which has affected the region's hydroclimate over the majority (96 %) of the 355 year study period. Our results further indicate that there is a pattern of seasonal evolution of precipitation anomalies during ENSO. However, considerable variability in the ENSO's influence is revealed: the strength of ENSO's influence was found to vary in time and space, and the different ENSO events resulted in varying precipitation anomalies. Additional research is needed to investigate how this variation in ENSO teleconnection is influenced by other factors, such as the properties of the ENSO events and other ocean and atmospheric phenomena. In general, the high variability we found in ENSO teleconnection combined with limitations of current knowledge, suggests that the adaptation to extremes in hydroclimate in mainland Southeast Asia needs to go beyond "predict-and-control" and recognise both uncertainty and complexity as fundamental principles.

1 Introduction

Extremes or changes in the mean state of climate can result in great duress to societies, especially during periods of prolonged drought or flood. A well-known source for droughts and floods on a global scale is the ocean–atmosphere coupled phenomena El Niño–Southern Oscillation (ENSO) (Cane, 2005; Ward et al., 2014). ENSO is

CPD
11, 5307–5343, 2015

an evolving phenomena (Trenberth and Shea, 1987) and it has become increasingly variable over recent decades (McGregor et al., 2013; Cai et al., 2014). Over mainland Southeast Asia, henceforth MSEA, ENSO explains a large part of the inter-annual hydrological variability (Juneng and Tangang, 2005), and many of the recent severe droughts and floods occurred during ENSO events (see e.g. Räsänen and Kummu, 2013). Changes in mainland Southeast Asia's hydroclimate variability is of great concern as the largely agrarian population and economy are growing rapidly (ADB, 2015; Pech and Sunada, 2008). Therefore regional livelihoods, economic and food security are strongly dependent upon hydroclimatic conditions (MRC, 2010; Keskinen et al., 2010). Despite such significance, however, the region's hydroclimate variability and its spatio-temporal connection to ENSO remains poorly understood.

Past research has shown that ENSO modulates precipitation, temperature and river flows over mainland Southeast Asia (Cook et al., 2012; Anchukaitis et al., 2015). Precipitation is known to decrease during warm phase (El Niño) events and increase during cool phase (La Niña) events (Juneng and Tangang, 2005; Singhrattna et al., 2005b; Räsänen and Kummu, 2013). The effect of ENSO has been reported to be stronger in the southern parts of mainland Southeast Asia, particularly so during the second year (i.e. decay year) of an event (Räsänen and Kummu, 2013; Juneng and Tangang, 2005). ENSO's correlation with precipitation is strongest in southern SEA, weakening towards the north and there are indications of opposite correlation between southern and northern areas (Räsänen and Kummu, 2013; Kiem et al., 2005). While El Niño events are associated with higher land surface temperature over the study region, La Niña events are accompanied by lower temperatures (Limsakul and Goes, 2008).

The relationship between ENSO and hydroclimate varies in time over MSEA. In general, during periods when hydrological conditions are below (above) average the effects of El Niño (La Niña) on precipitation are more severe (Kripalani and Kulkarni, 1997). However, precipitation analyses over Thailand show that the connection between precipitation and ENSO has become stronger in the post-1980 period (Singhrattna et al., 2005b). Variation in the relationship between ENSO and hydroclimate are also found

CPD
11, 5307–5343, 2015

in the river flows. The analyses of the Mekong River show stronger relationship between ENSO and river flow before the 1940s and after the late 1970s (Räsänen and Kummu, 2013; Darby et al., 2013). The changes in the relationship between ENSO and hydroclimate are linked at least to changes in ENSO's connection to different monsoon components. MSEA lies between the Indian summer monsoon (ISM) and western North Pacific summer monsoon (WNPSM) regions, and since late 1970s the relationship between ENSO and WNPSM has strengthened while the relationship between ENSO and ISM has weakened (Wang et al., 2008; Hsu et al., 2014).

Xu et al. (2013) reconstructed the multivariate ENSO index (MEI) using stable isotopes of Oxygen (^{18}O) from cross-dated tree rings of the Vietnamese cypress (*Fokienia hodginsii*). Their results illustrate the long term nature of ENSO's influence over the region, identifying at least 121 El Niño and 130 La Niña events between the years of 1605 and 2002. Other hydrological reconstructions also suggest long-term connection between ENSO and the regional hydroclimate, and make an unequivocal linkage between severe droughts and El Niño events (Buckley et al., 2007, 2010; Sano et al., 2008; Buckley et al., 2014).

While the linkage between ENSO and hydroclimate over MSEA has developed rapidly over past years, the spatial characteristics and long-term stationarity of this linkage is not yet well understood. The advancement of the knowledge in these two aspects would improve the scientific understanding of ENSO teleconnection and thus provide valuable information for adaptation to ENSO-related hydrological variability. Therefore, we aim to analyse the instrumental and proxy records of hydroclimate over the region to improve our understanding of the spatio-temporal variability of ENSO's influence on MSEA's largest river basins (Fig. 1). First we analyse instrumental records of precipitation over the period of 1980–2013 in order to investigate seasonal evolution and spatial variation in the effect of ENSO on precipitation over the MSEA, and second we analyse tree-ring based proxy records from two locations in MSEA that cover time period of 1650–2004 to investigate the long-term variations in ENSO teleconnection.

CPD
11, 5307–5343, 2015

2 Methodology

The spatial and temporal analysis of ENSO's influence on hydroclimate is divided into two parts: analysis of seasonal precipitation of the MSEA over the period 1980–2013, and analysis of proxy Palmer Drought Severity Index (PDSI) (for PDSI see Palmer, 1965) from two locations in MSEA over the period of 1650–2004. The precipitation analysis was aimed at improving the understanding of spatial and temporal patterns of ENSO-related precipitation anomalies and at understanding how strongly the hydroclimate in the locations of proxy PDSI data is related to ENSO. The precipitation was analysed using GPCC data (Schneider et al., 2015), the Multivariate ENSO index (MEI) (Wolter and Timlin, 1993, 1998) and correlation tests. Greater emphasis was given to the March–April–May season as PDSI proxy data are designed to describe the hydroclimate of that season. The analyses of proxy PDSI data were aimed at improving the understanding of how the ENSO-hydroclimate teleconnection in MSEA has varied in time. The proxy PDSI data were based on two tree-ring reconstructions from southern and northern Vietnam (Sano et al., 2008; Buckley et al., 2010; Cook et al., 2010), the unified ENSO proxy (McGregor et al., 2010) and on correlation and wavelet methods (e.g. Torrence and Compo, 1998). In addition we analysed the co-occurrence of extreme dry and wet years with ENSO events.

2.1 Precipitation analysis 1980–2013

The seasonal precipitation analysis was based on GPCC v.7 data (Schneider et al., 2015), which is an observation-based gridded climatological dataset with temporal coverage of 1901–2013 and spatial resolution of 0.5° (approx. 55 km at the equator). The analysis of precipitation was done on seasonal basis: June–July–August (JJA), September–October–November (SON), December–January–February (DJF), and March–April–May (MAM). The analysis was limited to the post-1980 period as previous research (Räsänen and Kummu, 2013) has reported a considerable decrease in the number of weather stations in the pre-1980 period. In addition, the post-1980 re-

CPD
11, 5307–5343, 2015

flects the recent period with stronger relationship between ENSO and hydrology (Räsänen and Kummu, 2013; Räsänen et al., 2013; Singhrattna et al., 2005b). We also considered CRU TS v.3.21 (Harris et al., 2014), and APHRODITE (Yatagai et al., 2009, 2012) precipitation for the analyses, but comparisons suggested that GPCC v.7 was the most suitable. CRU TS v.3.21 had major gaps in stations in the region of Myanmar and APHRODITE covers only a time period until 2007 and therefore does not capture most recent influential ENSO events. The comparison of GPCC v.7 and APHRODITE over their common period provided very similar results.

First the seasonal evolution of ENSO-related precipitation patterns was analysed. ENSO events are generally two year phenomena. They start to develop in spring, mature in early next year and decay in summer. Therefore the precipitation was aggregated into JJA(0), SON(0), DJF(0/1), MAM(1), JJA(1) and SON(1) seasonal sums and correlated with the time series of January–February–March value of MEI (NOAA, 2015b) from the second year of ENSO event (MEI_{JFM}). The JFM is the peaking period of ENSO events and thus the index values from these months represent the occurrence and strength of individual ENSO events (see e.g. Räsänen and Kummu, 2013; Singhrattna et al., 2005a). Pearson's correlation was used. The notations "0" and "1" in the names of the seasons denote the first year (i.e. developing year) and the second year (i.e. decaying) year of ENSO event, respectively. In a few occasions the ENSO event lasted three years and this third was denoted with "2". This correlation analysis provided maps of seasonal evolution of correlation between MEI_{JFM} and seasonal precipitation.

Second, we analysed the seasonal precipitation anomalies for each ENSO event and for each season over the MSEA. Anomalies were calculated as deviations from the 1980–2013 average precipitation and reported in percentages. This yielded seasonal precipitation anomaly maps of all El Niño and La Niña events in the period of 1980–2013. In addition we analysed the precipitation anomalies in more detail in the locations of proxy PDSI data in order to understand how strongly the hydroclimate at those locations is related to ENSO. This would provide understanding of how well the

CPD
11, 5307–5343, 2015

PDSI proxies are suited for analysing long-term ENSO teleconnection. The datasets used in the precipitation analysis are summarised in Table 1.

2.2 Proxy PDSI analysis 1650–2004

The temporal variability of ENSO's teleconnection to MSEA was analysed using two tree-ring based PDSI reconstructions developed by Sano et al. (2008) and Buckley et al. (2010), for northern and southern Vietnam, respectively. These two reconstructions marked the first two successful calibration-verification model schemes from tropical tree rings, both from the long-lived Vietnamese cypress (*Fokienia hodginsii*) of the family Cupressaceae regressed against the PDSI data set of Dai et al. (2004). In both cases the season of reconstruction was the three-month monsoon onset period of March–May, which is strongly influenced by the ENSO phenomenon (see Buckley et al., 2010, 2014). Together these two reconstructions cover a large portion of MSEA over Vietnam, Laos, Thailand and Cambodia. The PDSI reconstructions are referred to hereafter as $PDSI_{BDFH}$ (Buckley et al., 2010) and $PDSI_{MCC}$ (Sano et al., 2008) according to names of tree-ring study areas.

We used the Unified ENSO proxy (UEP), an index based on the ten most commonly used ENSO proxies that was originally published by McGregor et al. (2010) to describe ENSO behaviour over the 1650–2005 period. The original UEP is annual data and covers the time period from 1650 to 1977. We extended the UEP up to the year 2004 by using MEI in order to match the time period of the PDSI data. To do so we scaled the UEP variance to match the variance of MEI ($UEP \times \sigma_{MEI}/\sigma_{UEP}$) over the common period 1951–1977 for the annual average (July–June) of the two datasets, similarly to McGregor et al. (2010). The correlation between UEP and MEI over their common period is 0.81 ($p < 0.001$). The extended UEP is referred to hereafter as $ENSO_{UEP}$.

The $PDSI_{BDFH}$, $PDSI_{MCC}$ and $ENSO_{UEP}$ and their relationships were analysed using moving window correlation and wavelet methods (see e.g. Torrence and Compo, 1998; Grinsted et al., 2004). Moving window correlations were used to examine the temporal variation in the correlation between $ENSO_{UEP}$ and PDSI data. Pearson's correlation

CPD
11, 5307–5343, 2015

was used with a window width of 21 years. The statistical significance of correlations in each moving window was tested using the one-tailed Student's t test with 5 % significance level. Other window sizes were also tested but window of 21 years was proven most suitable for detecting continuous periods with statistically significant correlation.

The applied wavelet methods included the computation of wavelet power spectrum of single time series, as well as the cross-wavelet power spectrum and wavelet coherence spectrum of two time series together. The computations were done using the *WaveletComp* R-package developed by Rösch and Schmidbauer (2014). The wavelet power spectrum shows the time series in time-frequency space, which allows the examination of variations and their power in respect to their frequency and occurrence in time, while the cross-wavelet power spectrum shows where the variations of two time series have high common power in the time-frequency space. The wavelet coherence spectrum shows the coherence (i.e. localised correlation) between the two time series in time-frequency space, while the cross-wavelet power spectrum and the wavelet coherence spectrum also show the phase relationship between the two time series. In the case of correlated phenomena, the phase relationship is expected to be consistent in time. A more complete treatment of the wavelet methods can be found in Torrence and Compo (1998) and Grinsted et al. (2004).

The wavelet methods were used to identify, using the $PDSI_{BDFH}$, $PDSI_{MCC}$ and $ENSO_{UEP}$ data, the periods when ENSO had a stronger influence on the hydroclimate in MSEA. Two categories were used for this identification: *i. Strong ENSO-related variance*, *and ii. ENSO-related variance* in the hydroclimate of MSEA. These periods were defined according to regions in wavelet power, cross-wavelet power and coherence spectrum that were overlapping in time-frequency space and fulfilled specific criteria. The specific criteria are explained in detail in Table 2. The major difference between the two categories is that in the former the increase of the wavelet power is statistically significant. Non-significant ENSO-related variances are also analysed as they reveal periods with statistical relationship between ENSO and hydroclimate and provide an indication of the variations in the strength of ENSO teleconnection in MSEA. The wavelet

CPD
11, 5307–5343, 2015

analyses focused on periodicities from 2 to 10 years as they represent the frequencies of inter-annual ENSO variability. The statistical significance of the wavelet power and coherency was tested against white noise at the 5 % significance level.

In addition to wavelet analysis, we employed a variance analysis with an 11 year moving window in order to identify periods with high inter-annual variability in the time domain. This process also enabled us to see how well these periods correspond with the high-variability periods identified from wavelet analysis. We chose 11 years in order to capture the band of inter-annual variability without the decadal variability.

The co-occurrence of extreme dry and wet years with ENSO events was based on Gergis and Fowler (2009) multi-proxy ENSO event reconstruction over the period of 1525–2002. The extreme years were defined from PDSI data using 5th and 95th percentiles, which meant that 10 % of all years of PDSI data were defined as extreme. The co-occurrence of extreme years with warm and cool phase ENSO events was then identified by comparing the multi-proxy ENSO event reconstruction and extreme PDSI values. The datasets used in the proxy PDSI analysis are summarised in Table 1.

3 Results

3.1 Analysis of precipitation 1980–2013

The seasonal correlation analysis of precipitation and MEI_{JFM} shows different spatial correlation patterns for each season as shown in Fig. 2. The most distinctive feature of the seasonal correlations is the evolution of areas of statistically significant negative correlation from SON(0) to JJA(1) ($r < -0.339$, 5 % significance level) and the wide area of statistically significant positive correlation ($r > 0.339$, 5 % significance level) in northern regions in DJF(0/1). The negative (positive) correlation corresponds to reduced (increased) precipitation during El Niño and increased (reduced) precipitation during La Niña. During SON(0) the negative correlations are observed in the southern coastal regions in the west and east. In DJF(0/1) the areas negative correlation are

CPD
11, 5307–5343, 2015

pushed further south by areas of positive correlations. In MAM(1) the negative correlations are widespread in the study area. In JJA(1) the areas of negative correlations are observed only in western areas and in SON(1) the negative correlations have more or less disappeared. In addition, an interesting feature is also the areas of statistically significant positive correlation ($r > 0.339$, 5 % significance level) in the southern parts of the study area during the JJA(0) season.

The analysis of precipitation anomalies shows spatially varying anomaly patterns between ENSO events. This can be observed in Fig. 3 that shows the MAM(1) precipitation anomalies of eight El Niño and four La Niña events during the period of 1980–2013 and also in the Supplement that shows precipitation anomalies for all seasons for the same El Niño and La Niña events. In the case of El Niño events of 1982–1983, 1986–1987, 1991–1992, 1994–1995, 1997–1998, and 2009–2010 (Fig. 3a–h), the MAM(1) precipitation anomalies are widely negative in large parts of the study area. During the El Niño event of 2002–2003 the negative precipitation anomalies are smaller and positive anomalies are observed in some regions. During the El Niño event of 2006–2007 the precipitation anomalies are mainly positive and inconsistent with other El Niño events. In the case of La Niña events there is greater inconsistency in spatial patterns of MAM(1) precipitation anomalies than in the case of El Niño. During the 1998–1999 La Niña event, the MAM(1) precipitation anomalies are largely positive and cover the southern parts of the study area. During the 1988–1989 event, the positive precipitation anomalies are confined to the eastern part of the study area in Vietnam, in 2007–2008 the precipitation anomalies are more widespread in the southern parts of the study area but smaller, and in the 2010–2011 event, the positive precipitation anomalies are mainly in the western parts of the study area in Myanmar and in western Thailand.

The time series analysis of MAM(1) precipitation for the areas of $PDSI_{BDFH}$ and $PDSI_{MCC}$ (see locations in Fig. 3) show high correlation between precipitation and MEI_{JFM} and high consistency in the direction of precipitation anomalies during El Niño and La Niñ a events, as shown in Table 3. The Pearson's and Kendall's correlations for MAM(1) precipitation and MEI_{JFM} in the area of $PDSI_{BDFH}$ are −0.79 ($p \approx 0.000$)

CPD
11, 5307–5343, 2015

and −0.64 ($p \approx 0.000$), respectively. Similarly for the area of $PDSI_{MCC}$ the Pearson's and Kendall's correlations for MAM(1) precipitation and MEI_{JFM} are −0.69 ($p < 0.000$) and −0.5 ($p < 0.000$), respectively. During MAM(1+2) of El Niño events the precipitation anomalies were negative for the $PDSI_{BDFH}$ area in 80 % of the events and for the $PDSI_{MCC}$ area in 70 % of the events (Table 3). During MAM(1+2) of La Niña events the precipitation anomalies for the $PDSI_{BDFH}$ and $PDSI_{MCC}$ areas were positive in 100 % of the events (Table 3). The strong El Niño events stand out in the magnitude of precipitation anomalies: the precipitation anomalies during the second and third years are on average −32 and −24 %, varying in the ranges (−41, −14 %) and (−50, −1 %) for the areas of $PDSI_{BDFH}$ and $PDSI_{MCC}$, respectively.

3.2 Analysis of proxy PDSI 1650–2004

The precipitation analyses provided a good understanding of the hydroclimate and its relationship to ENSO in the areas of $PDSI_{BDFH}$ and $PDSI_{MCC}$. The $PDSI_{BDFH}$ and $PDSI_{MCC}$ were found to be well located in terms of areas affected by ENSO, and the hydroclimate of the MAM season, which the PDSI data also describes, showed high correlation with ENSO. Therefore, $PDSI_{BDFH}$ and $PDSI_{MCC}$ are considered as good proxies for analysing the long-term teleconnection in MSEA.

The correlation analysis between $ENSO_{UEP}$ and $PDSI_{BDFH}$ and $ENSO_{UEP}$ and $PDSI_{MCC}$ with moving windows in Fig. 4 revealed that the correlations vary in time and also differ between $PDSI_{BDFH}$ and $PDSI_{MCC}$. Statistically significant negative correlations ($p < 0.05$) can be observed for $PDSI_{BDFH}$ approximately during 93 % and for $PDSI_{MCC}$ approximately during 67 % of the study period. The longest period of no statistically significant correlation was observed for $PDSI_{MCC}$ during 1885–1948, which interestingly coincides with the period of highest correlation for $PDSI_{BDFH}$. The most recent period of statistically significant correlation started for both $PDSI_{BDFH}$ and $PDSI_{MCC}$ around the mid-20th century. In the early 90th century the correlation with $PDSI_{MCC}$ interestingly changes into a strong positive relationship. The periods with

CPD
11, 5307–5343, 2015

statistically significant correlation between PDSI data and $ENSO_{UEP}$ are also listed in Table 4.

The wavelet analyses in Figs. 5 and 6 also show a connection between ENSO and the hydroclimate of the region throughout the study period. The connection can be observed as a relatively consistent temporal distribution of statistically significant areas in the wavelet coherence spectrum of $ENSO_{UEP}$ and $PDSI_{BDFH}$ (Fig. 5d) and $ENSO_{UEP}$ and $PDSI_{MCC}$ (Fig. 5d). However, there are periods when there is no statistically significant coherence and the phase arrows point in inconsistent directions, for example from 1760s to late 1770s, suggesting no connection between ENSO and the hydroclimate.

The wavelet analyses of $PDSI_{BDFH}$ in Fig. 5 show seven periods with strong ENSO-related variance and four periods with ENSO-related variance in the hydroclimate. The periods strong ENSO-related variance coincide also with the overall increase in the variance as shown by the moving window analysis in Fig. 5b. For example, three periods with high variance are identified and these coincide with the periods of 1735–1750, 1871–1899 and 1960–1980 with ENSO-related variance (Fig. 5). In $PDSI_{BDFH}$ there are also three periods with significant increase in wavelet power that could not be associated with $ENSO_{UEP}$ (Fig. 5b). Thus in the region of $PDSI_{BDFH,}$ seven out of ten periods with statistically significant increase in wavelet power can be associated to ENSO. The identified periods with ENSO-related variance in $PDSI_{BDFH}$ are also listed in Table 4.

The wavelet analyses of $PDSI_{MCC}$ in Fig. 6 show two periods with strong ENSO-related variance and ten periods with ENSO-related variance in the hydroclimate (Fig. 6; Table 4). Many of these periods coincide with the general increase in the variance as shown by the moving window variance in Fig. 6b, for example in 1703–1745, 1829–1842 and in 1949–1958. Statistically significant increase in wavelet power of $PDSI_{MCC}$ can be observed also during the first half of 19th century (Fig. 6b), but its association with $ENSO_{UEP}$ is unclear. During this period both $ENSO_{UEP}$ and $PDSI_{MCC}$ show increase in wavelet power (Fig. 6a and b) and statistically significant coherence (Fig. 6d), but the phase arrows are pointing opposite to the general direction. The change in the direction of correlation was observed also in the analysis with mov-

CPD
11, 5307–5343, 2015

ing window correlation in Fig. 4. The identified periods with ENSO-related variance in $PDSI_{MCC}$ are also listed in Table 4.

The wavelet analyses also reveal that increased variance in ENSO does not always result in increased hydrological variance in MSEA. For example, the statistically significant increases in wavelet power of $ENSO_{UEP}$ in 1784–1795 (periodicities of about 5 and 8 years), 1901–1906 (periodicity of around 3 years), 1940–1955 (periodicities of about 4 and 6 years) and 1980–1989 (periodicity of 3–6 years) did not result in increase in wavelet power in $PDSI_{BDFH}$ (Fig. 5b). Similarly, the significant increases in wavelet power of $ENSO_{UEP}$ in 1784–1795 (periodicity of around 8 years) and 1915–1921 and 1981–1989 (periodicity of around 5 years) (Fig. 5a) did not result in increase in wavelet power of $PDSI_{MCC}$ (Fig. 6b). This suggests non-stationarity in the relationship between ENSO and hydroclimate over MSEA.

The analysis of extreme PDSI values in Figs. 5e and 6e shows that the majority of the most extreme dry and wet years occurred during ENSO events, particularly in the region of $PDSI_{BDFH}$. Altogether 18 years were defined as extremely dry and 18 years as extremely wet in $PDSI_{BDFH}$ and $PDSI_{MCC}$ using 5th and 95th percentiles. In the case of $PDSI_{BDFH}$, 13 (72 %) extremely dry years occurred during El Niño events and 13 (72 %) extremely wet years occurred during La Niña events. For $PDSI_{MCC}$, the respective figures are 6 (33 %) extremely dry years that occurred during El Niño events and 10 (56 %) extremely wet years that occurred during La Niña events. This indicates in general that in the region of $PDSI_{BDFH}$ both extremely dry and wet years tend to co-occur more often with ENSO events than in the region of $PDSI_{MCC}$.

When the results of the moving-window correlation analyses and the wavelet analyses of both $PDSI_{BDFH}$ and $PDSI_{MCC}$ are examined together as in Fig. 8 and Table 4, a more coherent picture can be drawn of ENSO's influence over MSEA. There is evidence of ENSO signal in the hydroclimate of MSEA approximately 96 % of the time over the 355 year study period, but the strength of this ENSO signal varies across time and space The wavelet analyses suggest that approximately during 52 % of the study period there was strong in ENSO-related variance and during 17 % ENSO-related vari-

CPD
11, 5307–5343, 2015

ance in the hydroclimate of the MSEA. The periods with ENSO-related variance in $PDSI_{BDFH}$ and $PDSI_{MCC}$ overlap each other relatively well, but there are also differences. For example, the strength, timing, length and continuity of the periods vary between $PDSI_{BDFH}$ and $PDSI_{MCC}$, consistent with spatial variation in the hydrological effects of ENSO in MSEA.

4 Discussion

The findings of this paper provide new information on the spatial distribution and temporal variability of ENSO's influence on the hydroclimate of MSEA. Evolution of statistically significant correlation patterns between precipitation and MEI_{DJF} was observed over MSEA over the period of 1980–2013. During the development phase of ENSO events in SON(1), areas of negative correlations are observed in several regions in MSEA. During the peaking months of ENSO events in DJF(1), these areas of negative correlation are then limited to the southernmost parts of the study area by areas of positive correlation in the north. During the decay phase of ENSO events in MAM(1), the majority of the MSEA is covered by negative correlation and the correlations are strong. In JJA(1) negative correlations exists only in eastern part of MSEA and in SON only small and scattered areas of correlation can be observed. The precipitation anomalies between different ENSO events were also found to vary considerably. Over the past 355 years an ENSO signal was observed approximately 96 % of the time, but its strength was found to vary in time and space. Approximately 56 % of the time, strong ENSO-related variance was observed in the hydroclimate. Furthermore, the majority of the extreme dry and wet years were found to co-occur with ENSO events, particularly in the southern parts of MSEA. These results point to a need for further research. In the following sections we further discuss the methodology, compare our findings with past research and suggest directions for future work as well as for adaptation to ENSO-related hydrological anomalies.

CPD
11, 5307–5343, 2015

4.1 On the methodology

The analysis of the long-term ENSO-hydroclimate relationship using two methods (moving window correlation and wavelets) and two hydroclimate proxies derived from tree rings ($PDSI_{BDFH}$ and $PDSI_{MCC}$) was found to be a useful approach. The two methods and two hydrological proxies revealed aspects of this relationship that neither of the methods or data could have achieved alone. For example, wavelet methods revealed statistical relationship between ENSO and hydroclimate where the moving window correlations did not (see e.g. Fig. 7). The two hydrological proxies complemented each other by capturing the spatially varying effects of ENSO and thus provided a more complete picture of the relationship between ENSO and hydroclimate.

However, there are certain limitations in the above approach in providing exact annual dating for the periods with connection between ENSO and hydroclimate. First, the moving window correlation was based on a window size of 21 years, resulting in ambiguity in the dating of the statistically significant periods. Second, the visual interpretation of the wavelet images involves a certain amount of subjectivity when multiple images are compared simultaneously. For example, subjective judgement was needed when the statistically significant areas in wavelet power, cross wavelet power and coherence spectrum images were of different size and not perfectly overlapping and when the phase arrows varied slightly from the expected direction. In order to minimise the errors from subjectivity, clear rules for consistent interpretation were developed and followed (see Methodology Sect. 2). Third, the size of statistically significant areas in wavelet images depended on parameters of the wavelet analysis. For example, the choice of statistical significance testing method affected the size of the statistically significant areas, which may change timing and duration of any such identified ENSO periods with so few years. Fourth, it is likely that the approach used was not able to capture all individual ENSO events that resulted in anomalies in hydroclimate. Despite these limitations, the results are based upon standard methods in time series analy-

CPD
11, 5307–5343, 2015

sis and are therefore considered to be reliable estimates of ENSO-related hydrological variability.

4.2 Comparison to earlier studies

The general finding that El Niño (La Niña) events result in drier (wetter) conditions over MSEA has been shown by past research (Juneng and Tangang, 2005; Kripalani and Kulkarni, 1997), and at more local scales in Thailand (Singhrattna et al., 2005b), and in the Mekong River basin (Räsänen and Kummu, 2013). These studies also suggest stronger correlation between ENSO and hydroclimate in central and southern parts of MSEA. The tree ring studies used here (Sano et al., 2008; Buckley et al., 2010) illustrate the strong inverse relationship between the reconstructed drought metric PDSI and ENSO, for both northern and southern Vietnam, respectively. Buckley et al. (2014) expands upon this discussion by using tree ring records from all across monsoon Asia and North America, illustrating that the dominant mode of climate variability across both sides of the Pacific is driven by ENSO-like variability, particularly at decadal scales (i.e., the Inter-decadal Pacific Oscillation or IPO – see Meehl and Hu (2006) and Buckley et al. (2010) for further details). Indeed, other tree ring sites from Thailand (Buckley et al., 2007) and Myanmar (D'Arrigo et al., 2011) confirm the strength of this relationship in these regions as well. The transition of the influence of ENSO to opposite sign from south to north was previously reported for the Mekong River basin (Räsänen and Kummu, 2013), and is supported by studies focusing on the upper reaches of the Mekong and Yangtze River basins (Kiem et al., 2005; Zhang et al., 2007). The past research provided either high resolution for a small area, or coarse resolution for a large area but not both, such that this work provides a more spatially accurate and uniform picture of the distribution of ENSOs influence, allowing comparison between different regions and seasons of MSEA. The research we present here confirms these past findings and provides an improved picture of the spatial and temporal distribution of ENSO's influence that allows regional and seasonal comparison.

CPD
11, 5307–5343, 2015

The variation in the hydroclimatic effects of ENSO events is less studied over MSEA. The variation in the magnitude and direction of annual precipitation and discharge anomalies during individual ENSO events are shown at least in the Mekong River basin (Räsänen and Kummu, 2013). These findings from the Mekong show that not all El Niño (La Niña) events resulted in negative (positive) precipitation and discharge anomalies. However, the study from the Mekong did not specifically analyse differences between individual ENSO events and seasons. The findings of the current research confirm the findings from the Mekong and provide a broader picture at seasonal and MSEA scales. Altogether, the findings of the current study show that the precipitation anomalies and their spatio-temporal patterns vary considerably between individual ENSO events, which makes reliable distinction between ENSO-related and non-ENSO-related rainfall anomalies very difficult.

The long-term relationship of ENSO and hydroclimate in MSEA has been shown to exist at centennial scales by several studies (Xu et al., 2013; Buckley et al., 2007, 2010; Sano et al., 2008), but the *variation* of the relationship of ENSO and hydroclimate has been studied only over the past hundred years or so. Studies conducted in Thailand (Singhrattna et al., 2005b) and the Mekong River basin (Räsänen and Kummu, 2013; Räsänen et al., 2013) report that the most recent periods of stronger relationship between ENSO and hydroclimate occurred during the beginning of the 20th century and lasted until the 1940s, while the second period began around the 1960s–1980s. The current research agrees with the findings from Thailand and the Mekong River Basin and suggests a period of weaker relationship between ENSO and hydroclimate during the 1930s–1950s in the Southern parts of the study area ($PDSI_{BDFH}$; see Figs. 1 and 7, and Table 4). But in the central and more northern part of the study area, the period of weak relationship lasted from the beginning of the 20th century until the late 1950s ($PDSI_{MCC}$; see Figs. 1 and 7, and Table 4). The differences in the timing of weak and strong periods may result from the different methodologies and locations of the studies, but they also strengthen our conclusion that the ENSO teleconnection over MSEA is

CPD
11, 5307–5343, 2015

highly variable across space and time. Furthermore, such variability has been evident for at least the past 355 years.

4.3 Future research directions and implications for adaptation

The findings of the current paper indicate considerable uncertainties in the effects of ENSO on hydroclimate and how this relationship develops through time. For example, clear patterns were found in the seasonal evolution of precipitation anomalies during ENSO events, but at the same time the precipitation anomalies and their spatio-temporal patterns were found to vary considerably between ENSO events. This leads to two potentially useful research directions related to ENSO. The first research direction would explore the physical characteristics (e.g. sea surface temperature, air pressure, wind and moisture fluxes patterns) of each ENSO events and how they translate into anomalies in hydroclimate in MSEA. For example, it is hypothesised that the placement of the descending limb of the Walker circulation could affect the ENSO teleconnection over MSEA (Singhrattna et al., 2005b). The second direction would explore how other climatic and oceanic phenomena interact with ENSO teleconnection in MSEA. For example, it is known that the Indian Ocean Dipole (IOD) affects the hydroclimate over MSEA (Darby et al., 2013) and there are good indications of the effect of the Pacific Decadal Oscillation (PDO) (Delgado et al., 2012). In addition, the current research discovered statistically significant positive correlation between precipitation and MEI_{JFM} in the northern regions of MSEA during DJF (0/1) season, but did not investigate it further. To our knowledge this phenomena has not been reported before and therefore there is need for further research.

The findings of this study also provide perspectives for adaptation to extremes in hydroclimate. The findings suggest some degree of statistical predictability of ENSO-related anomalies in hydroclimate, but at the same time the findings revealed large variation and thus uncertainties in the effects of ENSO in MSEA. It is well known that statistical approaches have severe limitations when it comes to predicting extreme events (see e.g. Nassim, 2010). Thus, given the high variability in the effects of ENSO,

CPD
11, 5307–5343, 2015

limitations in the current knowledge and statistical approaches we suggest exploration of adaptation approaches that embrace uncertainty and complexity and seek adaptation opportunities in multiple sectors and levels of society (see e.g. Resilience concept: Walker et al., 2004, 2013) while considering other ongoing environmental changes (Keskinen et al., 2010; Lauri et al., 2012; Pech and Sunada, 2008). For example, adaptation only through engineering solutions is likely to aggravate already existing challenges (e.g. Baran and Myschowoda, 2009). The suggested adaptation approaches could further benefit from analysis of the societal impacts of the identified historical events, and the coping mechanisms used to deal with them in the past (Nuorteva et al., 2010; Buckley et al., 2010).

5 Conclusions

Variability in hydroclimate affects various economic activities, local livelihoods and food security across mainland Southeast Asia. This paper aimed at improving the understanding of the variability in hydroclimate by investigating the spatial and temporal variability of ENSO teleconnection over the period of 1650–2013. The investigations were based on analyses of gridded precipitation data (1980–2013), proxy Palmer Drought Severity Index and proxy ENSO data (1650–2004). In so doing, we revealed that ENSO has affected the region's hydroclimate over the majority (96 %) of the 355 year study period and during half (56 %) of the time this effect was found to be strong. The precipitation anomalies were found to evolve during the development of ENSO events and they were at their strongest in the spring when the ENSO events decay. In addition, the majority of the extremely wet and dry years were found to have occurred during ENSO events, particularly in the southern parts of the study area. However, the findings suggest a high degree of variability in the effects of ENSO. The magnitudes and spatial patterns of precipitation anomalies varied between individual ENSO events and the strength of the long-term ENSO teleconnection varied in time and space. Our find-

CPD
11, 5307–5343, 2015

ings thus suggest high uncertainty in the effects of ENSO and limitations in the current knowledge and thus point out a need for further investigations.

In addition, the findings of the paper provide insights for adaptation to extremes in hydroclimate. Given, the high impact and variability of ENSO, and limitations in the current knowledge and predictive skill, holistic approaches to adaptation are recommended. Adaptation should embrace uncertainty, seek adaptation opportunities within multiple sectors and levels of society and consider climate-related adaptation as part of broader adaptation to ongoing social and environmental changes. Forecasting and engineering based approaches are likely to be inadequate and will likely create further challenges.

Data availability

The precipitation data (GPCC v.7) is available at DWD (2015), the Multi-variate ENSO Index at NOAA (2015b), the Unified ENSO Proxy at NOAA (2015c), the Multi-proxy ENSO Event Reconstruction at (NOAA, 2015d) and the PDSI proxies can be downloaded from (NOAA, 2015a).

The Supplement related to this article is available online at doi:10.5194/cpd-11-5307-2015-supplement.

Acknowledgements. T. A. Räsänen and V. Lindgren received funding from *Maa- ja vesitekniikan tuki ry*, J. H. A. Guillaume from Academy of Finland funded project NexusAsia (grant No. 269901), B. M. Buckley from NSF grants GEO 09-08971 and AGS 130-3976, and M. Kummu from Academy of Finland funded project SCART (267463).

CPD
11, 5307–5343, 2015

References

ADB: GMS Statistics, Asian Development Bank, Greater Mekong Subregion Core Environment Program, available at: http://www.gms-eoc.org/gms-statistics, last access: 6 July 2015.

Anchukaitis, K. J., Cook, B. I., Cook, E. R., Buckley, B. M., and Fa, Z.-X.: Mekong River flow reconstructed from tree rings, Geophys. Res. Lett., in press, 2015

Baran, E. and Myschowoda, C.: Dams and fisheries in the Mekong Basin, Aquatic Ecosyst. Health, 12, 227–234, 2009.

Buckley, B., Palakit, K., Duangsathaporn, K., Sanguantham, P., and Prasomsin, P.: Decadal scale droughts over northwestern Thailand over the past 448 years: links to the tropical Pacific and Indian Ocean sectors, Clim. Dynam., 29, 63–71, 2007.

Buckley, B. M., Anchukaitis, K. J., Penny, D., Fletcher, R., Cook, E. R., Sano, M., Nam, L. C., Wichienkeeo, A., Minh, T. T., and Hong, T. M.: Climate as a contributing factor in the demise of Angkor, Cambodia, P. Natl. Acad. Sci. USA, 107, 6748–6752, doi:10.1073/pnas.0910827107, 2010.

Buckley, B. M., Fletcher, R., Wang, S.-Y. S., Zottoli, B., and Pottier, C.: Monsoon extremes and society over the past millennium on mainland Southeast Asia, Quaternary Sci. Rev., 95, 1–19, doi:10.1016/j.quascirev.2014.04.022, 2014.

Cai, W., Borlace, S., Lengaigne, M., van Rensch, P., Collins, M., Vecchi, G., Timmermann, A., Santoso, A., McPhaden, M. J., Wu, L., England, M. H., Wang, G., Guilyardi, E., and Jin, F.-F.: Increasing frequency of extreme El Niño events due to greenhouse warming, Nat. Clim. Change, 4, 111–116, 2014.

Cane, M. A.: The evolution of El Niño, past and future, Earth Planet. Sc. Lett., 230, 227–240, 2005.

Cook, B. I., Bell, A. R., Anchukaitis, K. J., and Buckley, B. M.: Snow cover and precipitation impacts on dry season streamflow in the Lower Mekong Basin, J. Geophys. Res.-Atmos., 117, D16116, doi:10.1029/2012JD017708, 2012.

Cook, E. R., Anchukaitis, K. J., Buckley, B. M., D'Arrigo, R. D., Jacoby, G. C., and Wright, W. E.: Asian Monsoon Failure and Megadrought During the Last Millennium, Science, 328, 486–489, doi:10.1126/science.1185188, 2010.

D'Arrigo, R., Palmer, J., Ummenhofer, C. C., Kyaw, N. N., and Krusic, P.: Three centuries of Myanmar monsoon climate variability inferred from teak tree rings, Geophys. Res. Lett., 38, L24705, doi:10.1029/2011GL049927, 2011.

CPD
11, 5307–5343, 2015

Dai, A., Trenberth, K. E., and Qian, T.: A global dataset of Palmer drought severity index for 1870–2002: relationship with soil moisture and effects of surface warming, J. Hydrometeorol., 7, 1117–1130, 2004.

Darby, S. E., Leyland, J., Kummu, M., Räsänen, T. A., and Lauri, H.: Decoding the drivers of bank erosion on the Mekong river: The roles of the Asian monsoon, tropical storms, and snowmelt, Water Resour. Res., 49, 1–18, 2013.

Delgado, J. M., Merz, B., and Apel, H.: A climate-flood link for the lower Mekong River, Hydrol. Earth Syst. Sci., 16, 1533–1541, doi:10.5194/hess-16-1533-2012, 2012.

DWD: GPCC Full Data Reanalysis Version 7 (0,5° resolution), Deutscher Wetterdienst, Federal Ministry of Transport and Digital Infrastructure, , available at: ftp://ftp.dwd.de/pub/data/gpcc/html/fulldata_v7_doi_download.html (last access: 12 August 2015), doi:10.5676/DWD_GPCC/FD_M_V7_050, 2015.

Gergis, J. L. and Fowler, A. M.: A history of ENSO events since A. D. 1525: implications for future climate change, Climatic Change, 92, 343–387, doi:10.1007/s10584-008-9476-z, 2009.

Grinsted, A., Moore, J. C., and Jevrejeva, S.: Application of the cross wavelet transform and wavelet coherence to geophysical time series, Nonlin. Processes Geophys., 11, 561–566, doi:10.5194/npg-11-561-2004, 2004.

Harris, I., Jones, P. D., Osborn, T. J., and Lister, D. H.: Updated high-resolution grids of monthly climatic observations – the CRU TS3.10 Dataset, Int. J. Climatol., 34, 623–642, doi:10.1002/joc.3711 2014.

Hsu, H.-H., Zhou, T., and Matsumoto, J.: East Asian, Indochina and Western North Pacific Summer Monsoon – an update, Asia-Pac. J. Atmos. Sci., 50, 45–68, doi:10.1007/s13143-014-0027-4, 2014.

Juneng, L. and Tangang, F.: Evolution of ENSO-related rainfall anomalies in Southeast Asia region and its relationship with atmosphere–ocean variations in Indo-Pacific sector, Clim. Dynam., 25, 337–350, 2005.

Keskinen, M., Chinvanno, S., Kummu, M., Nuorteva, P., Snidvongs, A., Varis, O., and Västilä, K.: Climate change and water resources in the Lower Mekong River Basin: putting adaptation into the context, J. Water Clim. Change, 1, 103–117, doi:10.2166/wcc.2010.009, 2010.

Kiem, A., Geogievsky, M., Hapuarachchi, H., Ishidaira, H., and Takeuchi, K.: Relationship between ENSO and snow covered area in the Mekong and Yellow river basins, in: Proceedings of symposium S6 held in 7th IAHS Scientific Assembly, Foz do Iguacu, Brazil, 2005.

CPD
11, 5307–5343, 2015

Kripalani, R. H. and Kulkarni, A.: Rainfall variability over South-East Asia - Connections with Indian Monsoon and ENSO extremes: new perspectives, Int. J. Climatol., 17, 1155–1168, 1997.

Lauri, H., de Moel, H., Ward, P. J., Räsänen, T. A., Keskinen, M., and Kummu, M.: Future changes in Mekong River hydrology: impact of climate change and reservoir operation on discharge, Hydrol. Earth Syst. Sci., 16, 4603–4619, doi:10.5194/hess-16-4603-2012, 2012.

Limsakul, A. and Goes, J. I.: Empirical evidence for interannual and longer period variability in Thailand surface air temperatures, Atmos. Res., 87, 89–102, 2008.

McGregor, S., Timmermann, A., and Timm, O.: A unified proxy for ENSO and PDO variability since 1650, Clim. Past, 6, 1–17, doi:10.5194/cp-6-1-2010, 2010.

McGregor, S., Timmermann, A., England, M. H., Elison Timm, O., and Wittenberg, A. T.: Inferred changes in El Niño–Southern Oscillation variance over the past six centuries, Clim. Past, 9, 2269–2284, doi:10.5194/cp-9-2269-2013, 2013.

Meehl, G. A. and Hu, A.: Megadroughts in the Indian Monsoon Region and Southwest North America and a Mechanism for Associated Multidecadal Pacific Sea Surface Temperature Anomalies, J. Climate, 19, 1605–1623, doi:10.1175/JCLI3675.1, 2006.

MRC: State of the Basin Report 2010, Mekong River Commission, Vientiane, Lao PD R, available at: http://www.mrcmekong.org/assets/Publications/basin-reports/MRC-SOB-report-2010full-report.pdf (last access: 9 November 2015), 2010.

Nassim, N. T.: The Black Swan: The Impact of the Highly Improbable, 2nd edn., Random House Inc., New York, 2010.

NOAA: Monsoon Asia Drought Atlas (MADA) 2015a.

NOAA: Multivariate ENSO Index, National Oceanic and Atmospheric Administration, Earth System Research Laboratory, available at: http://www.esrl.noaa.gov/psd/enso/mei/ (last access: 9 November 2015), 2015b.

NOAA: 350 Year Unified ENSO Proxy Reconstruction. Originally published by McGregor et al (2010). Available at: National Centers for Environmental Information, National Oceanic and Atmospheric Administration, https://www.ncdc.noaa.gov/paleo/study/8732 (last access: 9 November 2015), 2015c.

NOAA: Multiproxy ENSO Event Reconstructions, Originally published by Gergis and Fowler 2009, Available at: National Centers for Environmental Information, National Oceanic and Atmospheric Administration, https://www.ncdc.noaa.gov/paleo/study/8408 (last access: 9 November 2015), 2015d.

CPD
11, 5307–5343, 2015

Nuorteva, P., Keskinen, M., and Varis, O.: Water, livelihoods and climate change adaptation in the Tonle Sap Lake area, Cambodia: learning from the past to understand the future, J. Water Clim. Change, 1, 87–101, doi:10.2166/wcc.2010.010, 2010.
Palmer, W. C.: Meteorological Drought, Research Paper No. 45, Office of Climatology US Weather Bureau, Washington DC, 65 pp., 1965
Pech, S. and Sunada, K.: Population growth and natural-resources pressures in the Mekong River Basin, AMBIO, 37, 219–224, 2008.
Räsänen, T. A. and Kummu, M.: Spatiotemporal influences of ENSO on precipitation and flood pulse in the Mekong River Basin, J. Hydrol., 476, 154–168, 2013.
Räsänen, T. A., Lehr, C., Mellin, I., Ward, P. J., and Kummu, M.: Palaeoclimatological perspective on river basin hydrometeorology: case of the Mekong Basin, Hydrol. Earth Syst. Sci., 17, 2069–2081, doi:10.5194/hess-17-2069-2013, 2013.
Sano, M., Buckley, B., and Sweda, T.: Tree-ring based hydroclimate reconstruction over northern Vietnam from Fokienia hodginsii: eighteenth century mega-drought and tropical Pacific influence, Clim. Dynam., 33, 331–340, 2008.
Singhrattna, N., Rajagopalan, B., Clark, M., and Krishna Kumar, K.: Seasonal forecasting of Thailand summer monsoon rainfall, Int. J. Climatol., 25, 649–664, 2005a.
Singhrattna, N., Rajagopalan, B., Kumar, K. K., and Clark, M.: Interannual and Interdecadal Variability of Thailand Summer Monsoon Season, J. Climate, 18, 1697–1708, 2005b.
Torrence, C. and Compo, G. P.: A practical guide to wavelet analysis, B. Am. Meteorol. Soc., 79, 61–78, 1998.
Trenberth, K. E. and Shea, D. J.: On the Evolution of the Southern Oscillation, Mon. Weather Rev., 115, 3078–3096, doi:10.1175/1520-0493(1987)115<3078:OTEOTS>2.0.CO;2, 1987.
Walker, B., Holling, C. S., Carpenter, S. R., and Kinzig, A. P.: Resilience, Adaptability and Transformability in Social–ecological Systems, Ecol. Soc., 9, 2004.
Walker, W. E., Haasnoot, M., and Kwakkel, J.: Adapt or perish: a review of planning approaches for adaptation under deep uncertainty, Sustainability, 5, 955–979, doi:10.3390/su5030955, 2013.
Wang, B., Yang, J., Zhou, T., and Wang, B.: Inter-decadal changes in the major modes of Asian-Australian monsoon variability: strengthening relationship with ENSO since the late 1970s, J. Climate, 21, 1771–1789, 2008.

CPD
11, 5307–5343, 2015

Ward, P. J., Eisner, S., Flörke, M., Dettinger, M. D., and Kummu, M.: Annual flood sensitivities to El Niño–Southern Oscillation at the global scale, Hydrol. Earth Syst. Sci., 18, 47–66, doi:10.5194/hess-18-47-2014, 2014.

Wolter, K. and Timlin, M. S.: Monitoring ENSO in COADS with a seasonally adjusted principal component index, in: Proceedings of the 17th Climate Diagnostics Workshop, Norman, OK, NOAA/NMC/CAC, NSSL, Oklahoma Clim. Survey, CIMMS and the School of Meteor., Univ. of Oklahoma, 52–57, 1993.

Wolter, K. and Timlin, M. S.: Measuring the strength of ENSO events - how does 1997/98 rank?, Weather, 53, 315–324, 1998.

Xu, C., Sano, M., and Nakatsuka, T.: A 400-year record of hydroclimate variability and local ENSO history in northern Southeast Asia inferred from tree-ring δ18O, Palaeogeogr. Palaeocl., 386, 588–598, doi:10.1016/j.palaeo.2013.06.025, 2013.

Yatagai, A., Arakawa, O., Kamiguchi, K., Kawamoto, H., Nodzu, M., and Hamada, A.: A 44-year daily gridded precipitation dataset for Asia based on a dense network of rain gauges, SOLA, 5, 137–140, doi:10.2151/sola.2009-035, 2009.

Yatagai, A., Kamiguchi, Arakawa, O., Hamada, A., Yasutomi, N., and Kitoh, A.: APHRODITE: Constructing a long-term daily gridded precipitation dataset for Asia based on a dense network of rain gauges, B. Am. Meteorol. Soc., 93, 1401–1415, doi:10.1175/BAMS-D-11-00122.1, 2012.

Zhang, Q., Xu, C.-y., Jiang, T., and Wu, Y.: Possible influence of ENSO on annual maximum streamflow of the Yangtze River, China, J. Hydrol., 333, 265– 274, 2007. 1

CPD
11, 5307–5343, 2015

Table 1. Description of the data sets used in the analyses of this study.

Analysis	Name	Data description	Source
Precipitation analysis 1980–2013	Precipitation	GPCC v.7. Observation-based monthly gridded climatological dataset with temporal coverage of 1901–2013 and spatial resolution of 0.5° (approx. 55 km at the equator).	Schneider et al. (2015)
	MEI_{JFM}	Multivariate ENSO index. Bi-monthly index based on sea level pressure, zonal and meridional components of the surface wind, sea surface temperature, surface air temperature and cloudiness data. JFM refers to index months of Jan–Mar that were used in this study.	Wolter and Timlin (1993) Wolter and Timlin (1998)
Proxy PDSI analysis 1650–2004	$PDSI_{BDFH}$	Tree-ring based Palmer Drought Severity Index reconstruction from Northern Vietnam describing Mar–May monsoon conditions with temporal coverage of 1250–2008.	Buckley et al. (2010)
	$PDSI_{MCC}$	Tree-ring based Palmer Drought Severity Index reconstruction from Southern Vietnam describing Mar–May monsoon conditions with temporal coverage of 1470–2004.	Sano et al. (2008)
	$ENSO_{UEP}$	Unified ENSO proxy. Proxy index based on the ten most commonly used ENSO proxies with temporal coverage of 1650–1977. In this study the Unified ENSO proxy was extended to cover the time period up to 2004 using MEI, similarly as in McGregor et al. (2010).	McGregor et al. (2010)
	Multi-proxy ENSO event reconstruction	Multi-proxy ENSO event reconstruction. An annual record of El Niño and La Niña events and their strength with temporal coverage of 1525–2002.	Gergis and Fowler (2009)

CPD
11, 5307–5343, 2015

Table 2. The identification criteria for periods with ENSO-related variance in hydroclimate. Two types of variance periods were identified from Unified ENSO proxy and Palmer Drought Severity Index (PDSI) proxy data: strong ENSO-related variance and ENSO-related variance in the hydroclimate. These periods were defined according to regions in wavelet power spectrum (WP), cross-wavelet power (CWP) and coherence spectrum (WC) that were overlapping in time-frequency space and fulfilled the criteria in the table. Variance period refers to period when ENSO had increased influence on the hydroclimate in mainland Southeast Asia.

Identification criteria	ENSO-related variance in the hydroclimate	Strong ENSO-related variance in the hydroclimate
WP of PDSI: increase in the power	✓	✓ Statistically significant ($p < 0.05$)
WP of $ENSO_{UEP}$: increase in the power	✓	✓
CWP: increase in the common power	✓	✓ Statistically significant ($p < 0.05$)
WC: statistically significant coherence ($p < 0.05$)	✓	✓
CWP and WC: phase arrows suggest consistent phase lock	✓	✓

CPD
11, 5307–5343, 2015

Table 3. ENSO events NOAA (2015b) and March–April–May precipitation anomalies in the areas of $PDSI_{BDFH}$ and $PDSI_{MCC}$ over the period of 1980–2013. Locations of areas are shown in Fig. 2. Strong ENSO events as in NOAA (2015b) are highlighted in bold.

Year	ENSO event	Precipitation anomaly for the $PDSI_{BDFH}$ area	Precipitation anomaly for the $PDSI_{MCC}$ area
1980		−11 %	−10 %
1981		−16 %	20 %
1982	**Strong El Nino1**	**−12 %**	**−12 %**
1983	**Strong El Nino2**	**−41 %**	**−30 %**
1984		4 %	−8 %
1985		9 %	−9 %
1986	**Strong El Nino1**	**4 %**	**19 %**
1987	**Strong El Nino2**	**−39 %**	**−27 %**
1988	El Nino3/**Strong La Nina1**	**−11 %**	**4 %**
1989	**Strong La Nina2**	**19 %**	**6 %**
1990		−7 %	18 %
1991	**Strong El Nino1**	**−23 %**	**−21 %**
1992	**Strong El Nino2**	**−39 %**	**−50 %**
1993	**Strong El Nino3**	**−14 %**	**−1 %**
1994	El Nino1	9 %	15 %
1995	El Nino2	−23 %	−20 %
1996		14 %	5 %
1997	**Strong El Nino1**	**10 %**	**1 %**
1998	**Strong El Nino2**/La Nina1	**−24 %**	**−7 %**
1999	La Nina2	68 %	37 %
2000	La Nina3	41 %	24 %
2001		25 %	31 %

CPD
11, 5307–5343, 2015

Table 3. Continued.

Year	ENSO event	Precipitation anomaly for the $PDSI_{BDFH}$ area	Precipitation anomaly for the $PDSI_{MCC}$ area
2002	El Nino1	−19 %	15 %
2003	El Nino2	7 %	−14 %
2004		−4 %	14 %
2005		−15 %	−20 %
2006	El Nino1	8 %	5 %
2007	El Nino2/La Nina1	22 %	4 %
2008	La Nina2	31 %	17 %
2009	**Strong El Nino1**	**46 %**	**3 %**
2010	**Strong El Nino2/Strong La Nina1**	**−33 %**	**−30 %**
2011	**Strong La Nina2**	**8 %**	**15 %**
2012		19 %	16 %
2013		−14 %	−7 %

CPD
11, 5307–5343, 2015

Table 4. Periods with evidence of ENSO teleconnection in mainland Southeast Asia over the period of 1650–2004. Correlation periods refer to periods with statistically significant correlation in moving window correlation-analysis (Fig. 4) and Periods with ENSO-related variance in hydroclimate refer to periods when ENSO had stronger influence on hydroclimate according to wavelet analyses (Figs. 5 and 6). Statistically significant periods ($p < 0.05$) are in bold.

Correlation periods			Periods with ENSO-related variance in hydroclimate			Evidence of ENSO teleconnection mainland Southeast Asia
$PDSI_{BDFH}$	$PDSI_{MCC}$	Combined	$PDSI_{BDFH}$	$PDSI_{MCC}$	Combined	
1667–1765	**1663–1684**	**1663–1814**	**1653–1644**	1655–1666	1653–1666	1663–1814
1767–1814	**1696–1716**	**1817–1940**	**1681–1689**	1681–1699	1681–1699	1817–2004
1817–1839	**1724–1752**	**1943–2004**	**1703–1721**	**1703–1745**	1703–1750	
1842–1940	**1762–1811**		**1735–1750**	1778–1785	1778–1785	
1943–2004	**1821–1884**		1794–1804	1796–1803	1794–1804	
	1949–2004		1829–1841	1829–1842	1829–1842	
			1849–1858	1866–1887	1849–1858	
			1871–1899	1899–1918	1866–1942	
			1904–1925	1933–1942	1947–1980	
			1926–1937	1947–1959	1992–2002	
			1960–1980	1966–1978		
			1992–2002	**1992–2002**		

CPD
11, 5307–5343, 2015

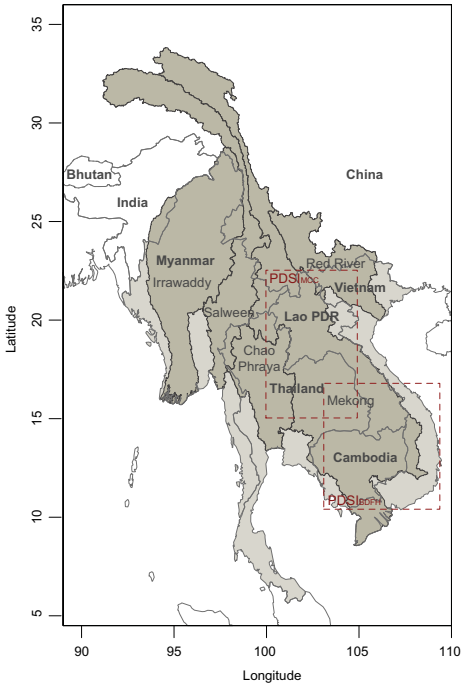

Figure 1. Map of the study area: mainland Southeast Asia. The spatial variability of ENSO's influence was analysed using annual precipitation data over the period of 1980–2013 with a focus on the area covering Myanmar, Thailand, Lao PDR, Vietnam and Cambodia and its largest river basins, the Irrawaddy, Salween, Chao Phraya, Mekong and Red River. The temporal variability of ENSO's influence was analysed using proxy Palmer Drought Severity Index (PDSI) data over the period of 1650–2004 with focus on two regions shown in the figure with rectangles denoting the $PDSI_{MCC}$ and $PDSI_{BDFH}$ reconstruction fields of Sano et al. (2008) and Buckley et al. (2010), respectively.

CPD
11, 5307–5343, 2015

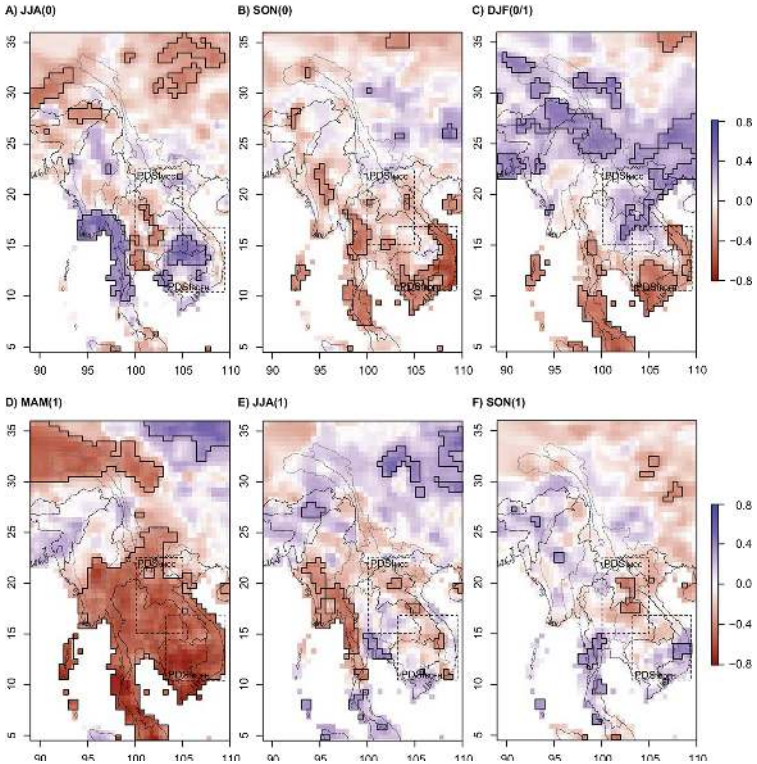

Figure 2. Map of correlation of January–February–March values of Multivariate ENSO index (MEI_{JFM}) and seasonal precipitation over the period of 1980–2013: **(a)** June–July–August (JJA (0)), **(b)** September–October–November (SON(0)), **(c)** December–January–February (DJF(0/1)), **(d)** March–April–May (MAM(1)), **(e)** June–July–August (JJA (1)) and **(f)** September–October–November (SON(1)). "0" denotes the first (i.e. developing) year and the "1" denotes the second (i.e. decaying) year of ENSO events. Black lines delimit areas of statistically significant correlation ($|r| > 0.339$, 5 % significance level).

CPD
11, 5307–5343, 2015

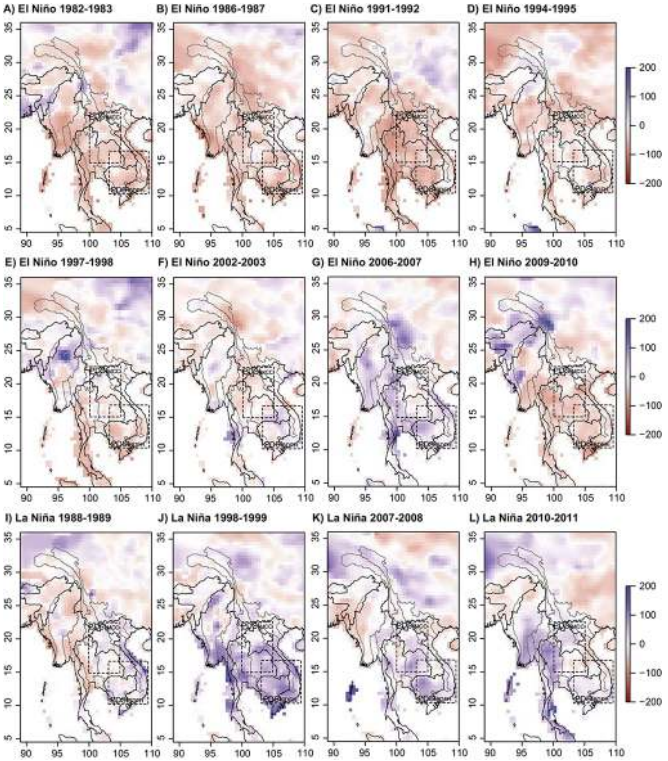

Figure 3. March–April–May precipitation anomalies [%] during the second year (MAM(1)) of **(a–h)** eight El Niño and **(i–j)** four La Niña events.

CPD
11, 5307–5343, 2015

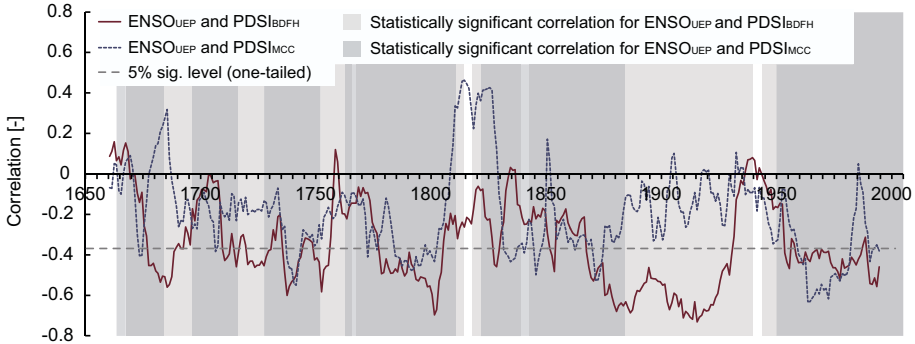

Figure 4. Correlations between $ENSO_{UEP}$ and $PDSI_{BDFH}$ and $ENSO_{UEP}$ and $PDSI_{MCC}$ using a 21 year moving window over the period of 1650–2004.

CPD
11, 5307–5343, 2015

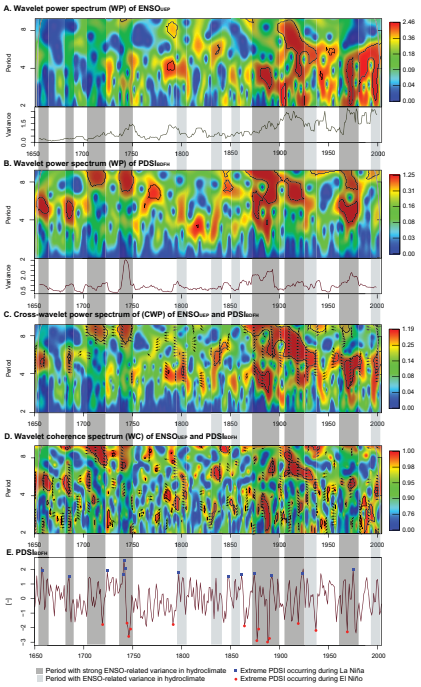

Figure 5. Wavelet analysis of the ENSO and $PDSI_{BDFH}$ over the period 1650–2004. Wavelet power spectrum of **(a)** $ENSO_{UEP}$ and **(b)** $PDSI_{BDFH}$, **(c)** cross-wavelet power spectrum and **(d)** wavelet coherence spectrum of $ENSO_{UEP}$ and $PDSI_{BDFH}$, and **(e)** time series of $PDSI_{BDFH}$. Tiles **(a)** and **(b)** also show total variances of time series calculated with a moving window of 21 years. Dark grey columns indicate periods with strong ENSO-related variance and the light grey columns indicate periods with ENSO-related variance in the $PDSI_{BDFH}$. Tile **(e)** also shows extreme PDSI values that occurred during ENSO events. Extreme values were defined from PDSI data as 5th and 95th percentiles.

CPD
11, 5307–5343, 2015

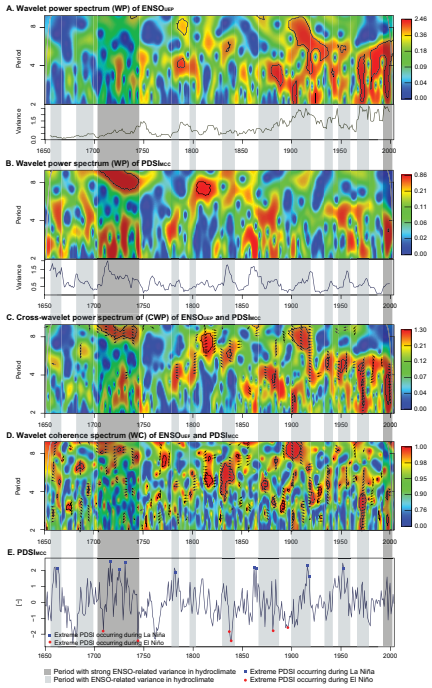

Figure 6. Wavelet analysis of the ENSO and $PDSI_{MCC}$ over the period 1650–2004. Wavelet power spectrum of **(a)** $ENSO_{UEP}$ and **(b)** $PDSI_{MCC}$, **(c)** cross-wavelet power spectrum and **(d)** wavelet coherence spectrum of $ENSO_{UEP}$ and $PDSI_{MCC}$, and **(e)** time series of $PDSI_{MCC}$. Tiles **(a)** and **(b)** show also total variances of time series calculated with moving window of 21 years. Dark grey columns indicate periods with strong ENSO-related variance and the light grey columns indicate periods with ENSO-related variance in the $PDSI_{MCC}$. Tile **(e)** also shows extreme PDSI values that occurred during ENSO events. Extreme values were defined from PDSI data as 5th and 95th percentiles.

CPD
11, 5307–5343, 2015

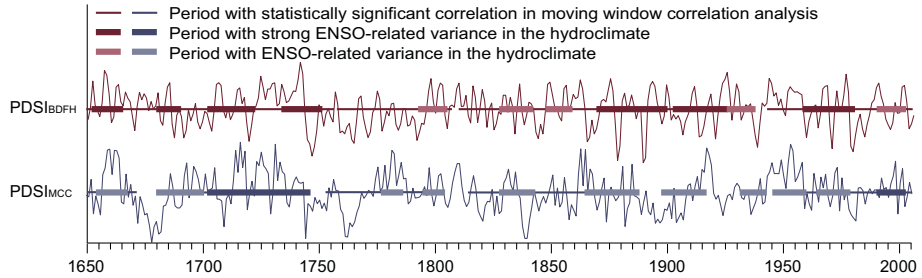

Figure 7. Periods with evidence of ENSO-related hydroclimate variability in mainland Southeast Asia over the period of 1650–2004. The periods with statistically significant correlation between the time series of $ENSO_{UEP}$ and $PDSI_{BDFH}$ and $PDSI_{MCC}$ are shown with thin horizontal lines and the periods with ENSO-related variance in $PDSI_{BDFH}$ and $PDSI_{MCC}$ are shown with thick horizontal lines.

CPD
11, 5307–5343, 2015